



1 **Linking Weather Regimes to the Variability of Warm-Season Tornado** 2 **Activity over the United States**

3 Authors: Matthew Graber¹, Zhuo Wang¹, & Robert J. Trapp¹

4 ¹Department of Climate, Meteorology, & Atmospheric Sciences, University of Illinois Urbana-
5 Champaign, Urbana, 61820, United States

6 *Correspondence to:* Zhuo Wang (zhuowang@illinois.edu)

7 **Abstract.** The contiguous United States (CONUS) experiences considerable interannual
8 variability in tornado activity. The high impacts of tornadoes motivate the need to better
9 understand the link between seasonal tornado activity and large-scale atmospheric circulation,
10 which may contribute to better seasonal prediction. We employed K-means clustering analysis of
11 500 hPa geopotential height (500H) daily anomalies from the ERA-5 reanalysis and identified
12 five warm-season weather regimes (WRs). Certain WRs are shown to strongly affect tornado
13 activity, especially outbreaks, due to their relationship with environmental parameters including
14 convective available potential energy (CAPE) and vertical wind shear (VWS). In particular, WR-
15 B, which is characterized by a three-cell wave-like pattern with an anomalous low over the
16 central-CONUS, is associated with enhanced CAPE and VWS in tornado-prone regions and
17 represents a tornado-favorable environment. Persistent WRs, those lasting for ≥ 5 consecutive
18 days, are associated with 76% of all tornado outbreaks (days with >10 EF-1+ tornadoes) since
19 1960, with a persistent WR-B accounting for about 30% of all tornado outbreaks. The impacts of
20 WR persistence on tornado activity anomalies, however, are found to be asymmetric: compared
21 to non-persistent WRs, persistent WRs amplify positive tornado activity anomalies but may not
22 further enhance negative tornado activity anomalies. An empirical model using WR frequency
23 and persistence captures the year-to-year variability of warm-season tornado days and outbreaks
24 reasonably well, including some years with high-impact outbreaks. Our study highlights the
25 potential application of WRs for better seasonal prediction of tornado activity.

26 **1 Introduction**

27 The contiguous United States (CONUS) experiences more tornadoes than anywhere else in the
28 world, leading to significant economic and life losses (NCEI, 2024). Tornado outbreaks (TOs)
29 are a primary contributor to these impacts, and the annual frequency has increased by 2.5 events
30 over the past 63 years (Brooks et al. 2014; Graber et al. 2024), particularly over the Southeast
31 U.S. (Gensini and Brooks, 2018; Graber et al., 2024; Moore, 2018; Moore and DeBoer, 2019). In
32 contrast, tornado days (TDs) have decreased in frequency at a rate of ~ 10 per decade since 1960
33 (Brooks et al. 2014; Graber et al. 2024), especially from March to September, and over the
34 southern Great Plains (Gensini and Brooks, 2018; Graber et al., 2024; Moore, 2018; Moore and
35 DeBoer, 2019). Embedded within these trends is large interannual variability, as evidenced by
36 the percent change, with respect to the previous year, in annual CONUS tornado reports over the
37 recent five years (2019-2023): +34.7%, -28.7%, +21.4%, -13.0%, and +24.5%, as well as by the
38 corresponding percent change in tornado fatalities: +320.0%, +80.9%, +36.8%, -77.9%, and
39 +260.9% (Storm Prediction Center, 2024). Such variability affects the situational awareness and



40 vulnerability of the populations, especially those that are disadvantaged. It also complicates
41 decision making and resource management by key stakeholders across multiple sectors. In
42 addition, exposure to future tornadoes is increasing with growing urban areas (Ashley and
43 Strader, 2016; Strader et al., 2017, 2024). These and other impacts motivate the efforts to better
44 understand the variability of tornado activity over the seasonal and longer time scale, which
45 would ultimately contribute to improved prediction of tornado activity.

46 Some variability of tornado activity can be attributed to low-frequency climate modes (Miller et
47 al., 2022; Niloufar et al., 2021; Thompson and Roundy, 1998; Vigaud et al., 2018). For example,
48 Lee et al. (2016) found that La Niña (El Niño) years typically coincide with increases (decreases)
49 in tornado activity in tornado-prone regions over the United States due to ENSO effects on the jet
50 streams (Cook et al., 2017). Additionally, a positive (negative) phase of the Arctic Oscillation
51 (AO) combined with a La Niña (El Niño) may increase (decrease) in tornado activity (Tippett et
52 al., 2022). Tornado activity can also be modulated by anthropogenic climate change (ACC),
53 either indirectly via changes in climate modes, such as through an increase in consecutive La
54 Niña years in a warming climate (Geng et al., 2023), or/and directly via changes in relevant
55 atmospheric conditions. For example, increasing greenhouse gas concentrations are projected to
56 lead to a moister atmosphere, especially in the lower troposphere, which in turn contributes to
57 higher convective available potential energy (CAPE) (Trapp et al., 2007). Diffenbaugh et al.
58 (2013) showed that climate models project a robust increase in the number of days with high
59 CAPE coinciding with high vertical wind shear (VWS) in the eastern U.S., two important
60 parameters for tornado-favorable environments (Brooks et al., 2003; Mercer and Bates, 2019;
61 Rasmussen and Blanchard, 1998; Thompson et al., 2012).

62 Variability of synoptic-scale circulations provides another means of explaining tornado activity.
63 Conductive synoptic-scale circulation anomalies for TOs in the United States show a trough-ridge
64 pattern over the central- to eastern-CONUS, while non-TOs usually feature more zonal flow and
65 weaker relative vorticity (Mercer et al., 2012). In particular, Cwik et al. (2022) performed rotated
66 EOF analysis of 500-hPa geopotential height associated with historic May TOs and identified
67 three circulation patterns. The three circulation patterns are all characterized by a trough feature
68 over the central to eastern U.S. While their study concludes that the synoptic patterns associated
69 with TOs remain the same over time, there is partial variability in the locations of TOs on
70 multidecadal scales. Additionally, mesoscale processes also affect tornadoes, especially weak or
71 isolated tornado events (e.g., tornadogenesis in non-supercellular storm modes associated with
72 mesoscale boundaries; see Wakimoto and Wilson, 1989).

73 In this study, we will investigate the link between the synoptic-scale circulation and tornado
74 activity using the concept of weather regimes (WRs). Different from EOF analysis, WRs
75 identified using K-means clustering analysis are not required to be orthogonal to each other,
76 which can more flexibly represent various recurrent synoptic-scale circulation patterns. Previous
77 studies suggest that WRs represent a finite number of equilibrium states of the climate system
78 (Charney and DeVore, 1979; Hannachi et al., 2017; Michelangeli et al., 1995). Their spatial



79 patterns are determined by the internal dynamics of the atmosphere, while their frequencies and
80 persistence may be modulated by climate modes or external forcings such as ACC (Corti et al.,
81 1999). The WR framework thus has a strong dynamic basis. Additionally, unlike Cwik et al.
82 (2022)'s study, which focuses on circulation patterns conditioned on major TOs, our
83 identification of WRs is independent of TOs. This approach allows us to examine WRs that
84 facilitate or hinder tornado activity, providing more comprehensive information for potential
85 forecasting applications. Furthermore, we will examine environmental conditions relevant to
86 tornado development, such as CAPE and VWS (Brooks et al., 2003; Mercer and Bates, 2019;
87 Rasmussen and Blanchard, 1998; Thompson et al., 2012), which will help us better understand
88 the link between WRs and tornado activity.

89 WRs were used previously to investigate sub-seasonal variability of tornado activity, and a
90 skillful WR-based, hybrid model was developed for the sub-seasonal prediction of tornado
91 activity in the month of May (Miller et al. 2020). Year-round WRs (Lee and Messori, 2024) have
92 also been used and found to have statistically significant relationships with tornado activity in all
93 months except June-August (Tippett et al. 2024) although without any consideration of WR
94 persistency. This helps motivate our focus herein on the warm-season tornado activity and its
95 interannual variability. We will test the hypothesis that the interannual variability of warm-
96 season tornado activity is modulated by WR frequency and persistence. A better understanding
97 of the possible links between WRs and tornado activity may contribute to improved seasonal
98 prediction of tornado activity.

99 **2 Data and Methodology**

100 **2.1 ERA-5 reanalysis data**

101 500 hPa geopotential heights (500H) and parameters, including most unstable CAPE
102 (MUCAPE), 10m and 500 hPa winds, and convective precipitation (CP), from the ERA-5
103 reanalysis dataset (Hersbach et al., 2020) were analyzed over the CONUS [24 – 55° N, 130 –
104 60° W] using the native 0.25° × 0.25° (latitude × longitude) resolution. Since the tornadic
105 storms leading to TOs tend to initiate between 18 and 00 UTC after sufficient atmospheric
106 destabilization from surface heating (Cwik et al., 2022), 500H at 21 UTC was used to represent
107 the daily circulation patterns. Daily maximum values of MUCAPE and at each grid point were
108 used to represent the daily peak instability and to avoid too many near-zero CP values in a daily
109 mean. The 0-6 km bulk wind shear (S06), or deep-layer shear, was estimated at each grid point
110 and 3-h interval as the magnitude of the vector difference between the 500 hPa and 10 m winds.
111 The daily mean S06 was then determined at each ERA-5 grid point. Following Graber et al.
112 (2024), all analyses were conducted over the period 1960-2022, and focused specifically on the
113 warm season, defined as April to July, which is peak season of tornado activity.

114 **2.2 Weather Regimes**



115 To identify weather regimes, the seasonal cycle, defined as the long-term mean of 21 UTC 500H
116 at each grid-point for each calendar day, was removed. The 500H data were then detrended by
117 removing the linear trend of the warm-season 500H averaged over the entire Northern
118 Hemisphere (Fig. S1). The detrending approach removed the positive trend of hemispheric mean
119 500H caused by climate change while preserving the spatial patterns and potential changes of
120 WR frequency or persistence. K-means clustering analysis was then applied to the 500H daily
121 anomalies over the CONUS, and the number of clusters was determined as five using the elbow
122 method (Miller et al. 2020; Kodinariya and Makwana 2013). A persistent WR was defined as a
123 WR lasting for ≥ 5 consecutive days.

124 **2.3 Tornado Reports**

125 Tornado reports were obtained from the NOAA Storm Prediction Center Severe Weather
126 Database. These reports are georeferenced with time, date, and EF/F rating. TDs were defined as
127 any day with ≥ 1 EF/F-1+ tornadoes, and TOs were defined as any day with >10 EF/F-1+
128 tornadoes. The >10 threshold provides a larger sample size than higher thresholds but has a
129 similar trend as >20 or >30 thresholds (Graber et al. 2024). Early reporting in the 1960s has
130 known biases, and EF/F-0 reports were not included due to their reporting uncertainty (Brooks et
131 al., 2014; Trapp, 2013). Despite the increase in weak tornado reports in the 1990s due to the
132 deployment of the NEXRAD radar system (Bieringer and Ray, 1996), this trend is not reflected
133 in TDs.

134 The TD probability anomalies (P_a) were calculated for each WR as follows:

$$135 P_a = \frac{P_i - P_c}{P_c} \times 100 \quad (1)$$

136 where P_c is the climatological mean TD probability and was calculated as the total number of
137 TDs divided by the total number of days in the warm-season from 1960-2022, and P_i represents
138 the TD probability for WR- i (i.e., the number of TDs for WR- i divided by the total WR- i days).
139 WRs that are (are not as) conducive for TDs would have probabilities above (below) the
140 climatological mean and thus positive (negative) probability anomalies. The probability
141 anomalies of TOs and the probability anomalies associated with persistent and non-persistent
142 WRs were calculated similarly.

142 **2.4 Empirical model for tornado activity**

143 Using WR frequency and tornado probabilities for both persistent (subscript p) and non-
144 persistent (subscript np) WRs, we developed an empirical model to assess the relationship
145 between the variability of seasonal tornado activity and WRs:

$$146 TI(t) = \sum_{i=1}^5 f(i,t)_p \times P_{i,p} + \sum_{i=1}^5 f(i,t)_{np} \times P_{i,np} \quad (2)$$

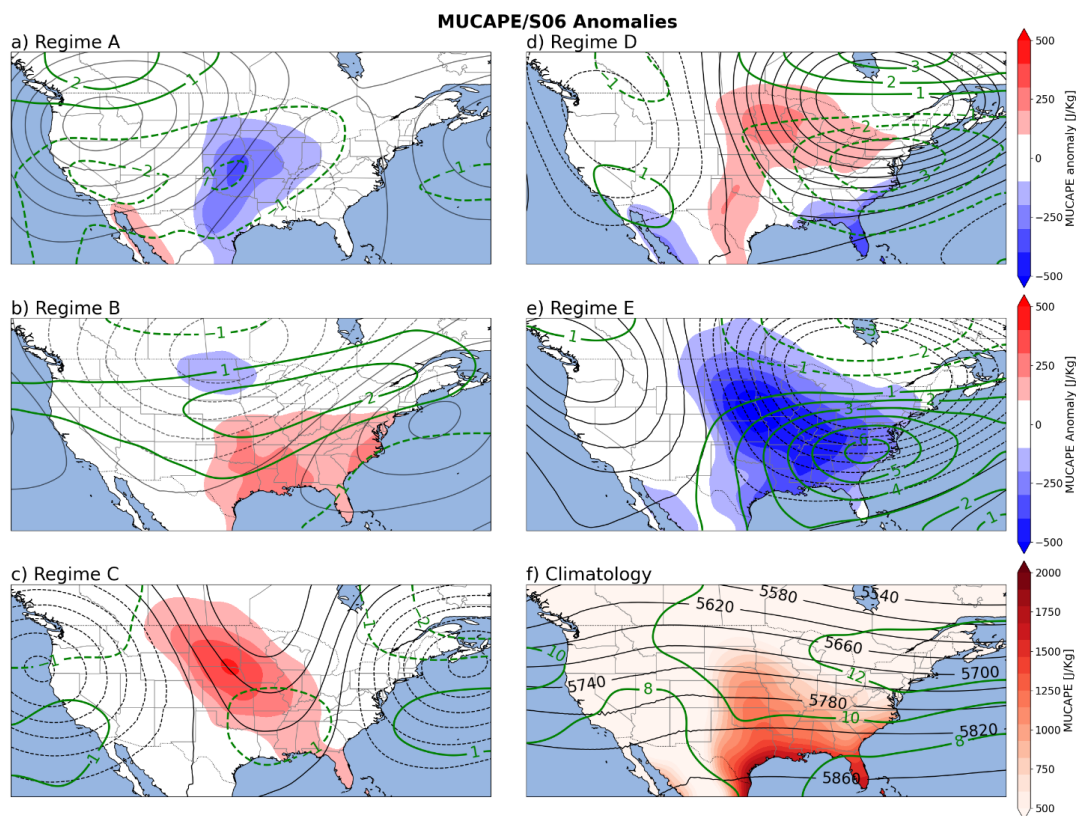


146 where $TI(t)$ denotes a tornado index for year t . The model takes the count of WR- i days ($f(i, t)$)
147 for year t and multiplies it by the tornado probability corresponding to WR- i ($P(i)$). The WR
148 count is a function of regime (i) and year (t). The WR tornado probability is only a function of
149 regime (i) and represents the likelihood that a TD will occur. Probabilities are assessed for
150 persistent and non-persistent WRs separately, under the hypothesis that persistent WRs
151 contribute to stronger TD or TO anomalies (Miller et al., 2020; Trapp, 2014). Spearman Rank
152 correlation is used to compare the modeled and observed tornado indices.

153 3 Weather Regimes and Tornado Activity

154 The composite mean 500h anomalies for each WR are shown in Fig. 1, ordered with decreasing
155 frequency of occurrence. WR-A is the most frequent regime and is characterized by an
156 anomalous high over the west-central-CONUS and a weak anomalous low over the Southeast.
157 WR-B and WR-C are both characterized by a three-cell wave pattern, with negative and positive
158 500h anomalies over the central-CONUS, respectively. WR-D and WR-E are west-east dipole
159 patterns that nearly mirror each other. These WRs have some spatial similarities to the year-
160 round WRs found by Lee and Messori, (2024), with WR-A reflecting a Pacific Trough, WR-B
161 and WR-D showing warm and cool phases of a Pacific Ridge associated with ENSO, and WR-E
162 reflecting an Alaskan Ridge.

163 The potential links between these WRs and tornado activity are indicated by MUCAPE and S06
164 (Fig. 1a-e). Composite anomalies of these parameters were calculated by subtracting the
165 corresponding climatological mean (Fig. 1f) from the composite mean associated with each WR.
166 The high values of the climatological MUCAPE across the central- and southeastern CONUS are
167 connected to the physical geography of North America (Brooks et al., 2003; Trapp, 2013) and
168 the warm-season climatological mean 850-hPa circulation, with southerly winds transporting
169 heat and moisture into the central-CONUS (Mercer and Bates, 2019). The climatological S06 is
170 characterized by high values over the eastern-CONUS, which are tied to the midlatitude jet
171 stream. With an anomalous high over the west-central-CONUS and an anomalous low over the
172 Southeast, WR-A favors anomalously low MUCAPE and S06 relative to climatological means.
173 In contrast, the anomalous low over central North America and the anomalous high over the
174 southeastern U.S. in WR-B imply enhanced westerly flow and increased moisture and warm-air
175 transport from the Gulf, leading to positive S06 and MUCAPE anomalies in southeastern U.S. In
176 WR-C, the anomalous low over western North America and the anomalous high over central
177 North America imply enhanced southerly flow and increased moisture and heat transport leading
178 to positive MUCAPE anomalies in the central U.S., which overlap with reduced S06 south of the
179 anomalous high. For WR-D, the anomalous high over the eastern CONUS and the anomalous
180 low over the western CONUS imply enhanced southerly flow and increased moisture and heat
181 transport, consistent with positive MUCAPE anomalies in the central U.S., while S06 decreases
182 in the south of the anomalous high and increases in the north. WR-E, in contrast to WR-D,
183 implies reduced southerly flow and decreased moisture and warm-air transport and is associated
184 with negative MUCAPE anomalies in the central U.S., but S06 increases substantially over the
185 Southeast.



186

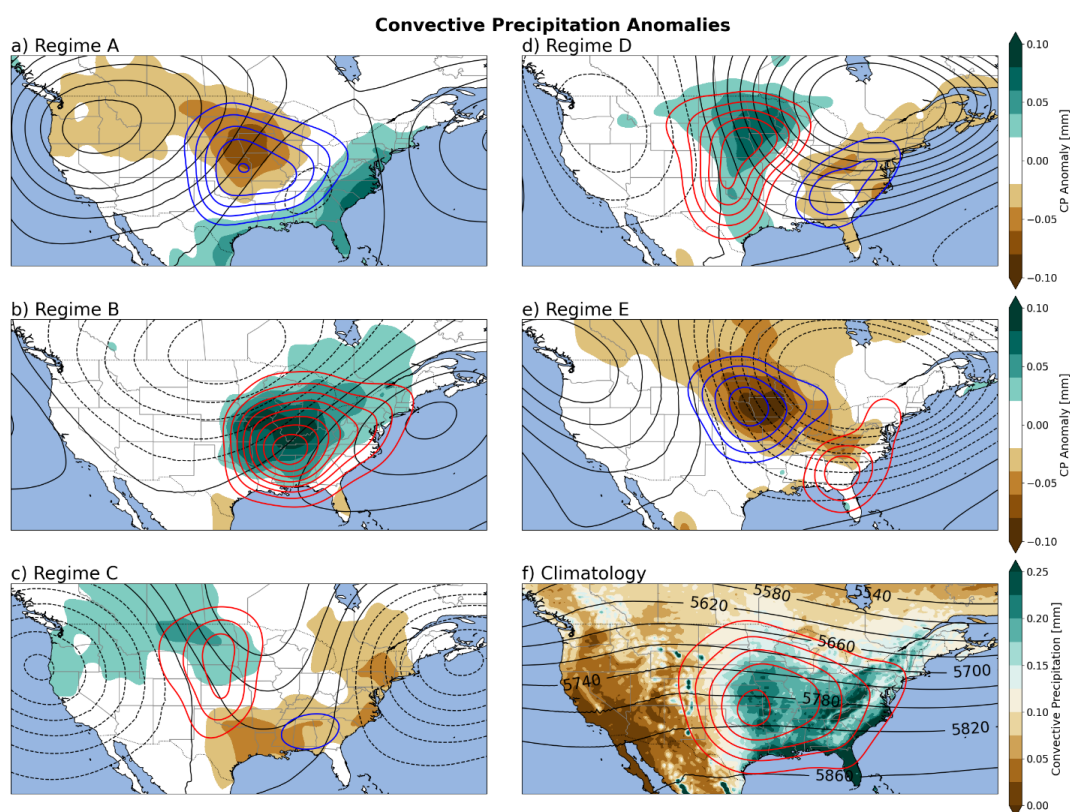
187 **Figure 1:** (a-e) Composite anomalies of 500H (black contours, +/- 10 m) for each warm-season WR and
 188 corresponding anomalies of daily maximum MUCAPE (units: J Kg^{-1} ; color fill) and daily mean S06 (units: m s^{-1} ;
 189 green contours); (f) Warm-season climatology of 500H (black contours), daily maximum MUCAPE (color fill) and
 190 daily mean S06 (green contours).

191 The WR-tornado activity link is illustrated by the composite anomalies of TD probability and CP
 192 for each WR. The climatological TD probability and CP are also shown (Fig. 2f) for reference.
 193 Here TD probability anomalies are evaluated following Eq. 1 with respect to P_c at each grid
 194 point. Convective-storm occurrences can be approximated using CP. Convective storms are a
 195 necessary but insufficient condition for tornadoes, so more CP does not necessarily lead to more
 196 tornadoes, but less CP likely means reduced tornado activity (Tippett et al., 2014). CP anomalies
 197 collocate well with the MUCAPE anomalies (Fig. 1) since non-zero CAPE is generally necessary
 198 for deep convection, but CP also includes information about convection initiation. WR-A has
 199 negative TD anomalies in the central-CONUS, where negative anomalies in CP and
 200 MUCAPE/S06 are also present. Positive TD anomalies in the Southeast and Midwest of WR-B
 201 are collocated with positive anomalies in CP, MUCAPE, and S06. Despite the negative S06
 202 anomalies, positive TD anomalies occur in the central Great Plains in a region of positive
 203 MUCAPE and CP anomalies for WR-C. Weak, negative TD anomalies in association with WR-
 204 C are found in the Southeast where negative CP anomalies are present. Positive (negative) TD



205 anomalies in WR-D over the central-CONUS are collocated with positive (negative) CP and
206 MUCAPE anomalies, and reduced S06 (Fig. 1d) also contributes to the negative TD anomalies in
207 the Southeast. Finally, negative TD anomalies occur in the central-CONUS, collocated with
208 negative anomalies of MUCAPE and CP associated with WR-E, while positive TD anomalies
209 occur in the Southeast despite reduced MUCAPE. The latter can probably be attributed to the
210 strong positive anomalies in S06 and may be possibly linked to tropical cyclones (Figs. 1e and
211 2e). However, given the low climatological TD probability in the Southeast (Fig. 2f), the
212 absolute changes in TD days may not be high. Overall, the distribution of TD anomalies shows a
213 good agreement with CP and MUCAPE anomalies of the same sign, and S06 seems to play a
214 secondary role in most regions.

215



216

217 **Figure 2:** a-e): Significant composite anomalies of daily maximum CP rate (units: mm h⁻¹; shading) at each grid
218 point (green/brown filled contours) for each WR A-E days with TD probability anomalies (contour intervals: +/- 10
219 %; red and blue colors represent positive and negative values, respectively) and 500H for each WR (black contours:
220 +/- 10 m); (f) Climatology of daily maximum CP (shading), 500H (black contours), and tornado day probability (red
221 contours). Significance is tested using Student's t-test, and anomalies with p-values ≤ 0.05 are regarded as significant.

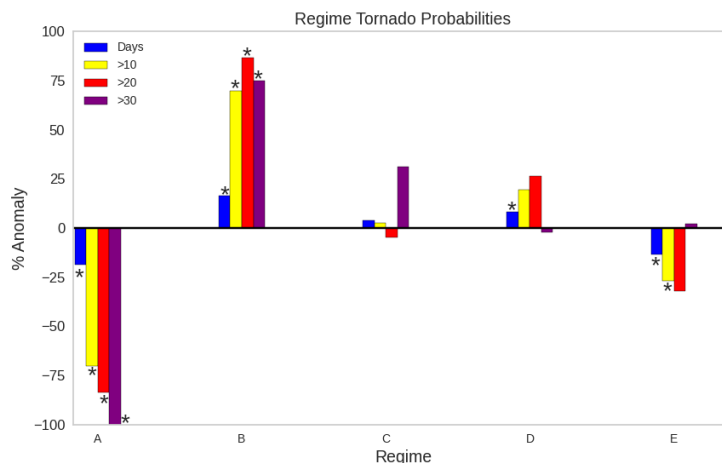
222 The link between WRs and geospatially aggregated tornado activity is summarized in Fig. 3 for
223 different regions. There are a total of 4348 warm-season TDs from 1960-2022, therefore $P_c \approx$



224 56.5%. TD probability is enhanced for WR-B and WR-D, with probability anomalies of **16.5%**
 225 and **8.2%**, respectively (corresponding to TD probabilities of **65.9%** and **61.3%**; Fig. 3). For
 226 reference, these are associated with large positive TD probability anomalies in the Southeast and
 227 central-CONUS, respectively (Fig. 2). TD probability is reduced for WR-A and WR-E,
 228 associated with negative tornado-report anomalies across the central-CONUS (Fig. 2). The TD
 229 probability anomaly associated with WR-C is close to zero (Fig. 3), which can be attributed to
 230 the cancellation between the opposite anomalies in the Southeast and central-CONUS (Fig. 2).

231 There are 415 warm-season TOs from 1960-2022, therefore $P_c = 5.4\%$. In general, the TO
 232 probabilities have a stronger signal than TDs (yellow bars in Fig. 3). For TOs, WR-A has the
 233 strongest negative signal with a **-70.01%** anomaly while WR-B has the strongest positive signal
 234 with a **+69.81%** anomaly (Fig. 3). The TO anomalies are consistent with the analysis in Figs. 1-
 235 2, in which WR-A (WR-B) showed reduced (enhanced) MUCAPE, S06, and CP over the central
 236 and Southeast CONUS. The TO probability associated with WR C is around the climatological
 237 mean. WR-D has a positive, but not significant anomaly of TO probability (**+19.56%**; Fig. 3),
 238 which is consistent with enhanced MUCAPE and CP over the central-CONUS (Figs. 1d&2d).
 239 WR-E is associated with a negative TO probability anomaly, which can be linked to the reduced
 240 tornado activity over the central-CONUS (Fig. 2). Further analysis reveals that roughly **83%** of
 241 all TOs occur during a WR-B, C, or D.

242 We also checked TOs using >20 and >30 tornadoes thresholds (red and purple bars in Fig. 3).
 243 The analysis based on the >20 threshold yields similar results as that defined based on the >10
 244 threshold. Although WR-A and WR-B demonstrate significant and consistent signals for days
 245 with >30 tornadoes, the other WRs exhibit contrasting signals for the >10 and >30 thresholds.
 246 This could be due to the small sample size of TOs when using the >30 threshold, and those
 247 anomalies are not significant.



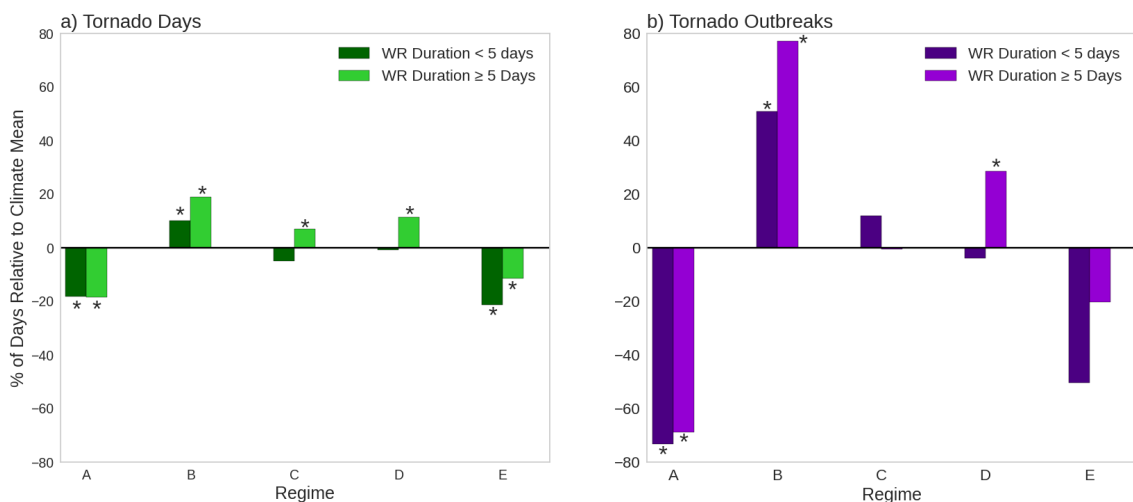
248

249 **Figure 3:** Tornado probability anomalies for days with > 0, > 10, > 20, & > 30 tornadoes for each WR in the
 250 CONUS (see Eq. 1 and the related discussion). Anomalies above the 95 % confidence level based on the Monte
 251 Carlo testing (with 10,000 resampling) are regarded as significantly different from zero and marked with an asterisk.



252 Next we compare persistent and non-persistent WRs to test the hypothesis that persistent regimes
253 amplify the TD/TO probability anomalies. Persistent WRs are defined as those lasting for at least
254 5 days. The comparison of the TD probability anomalies between persistent and non-persistent
255 WRs (Fig. 4a) does not fully support our hypothesis. Although persistent WR-B and WR-D are
256 associated with a stronger positive anomaly in TD probability than their non-persistent
257 counterparts, the negative TD probability anomalies are about the same for persistent and non-
258 persistent WR-A, and persistent WR-E shows an even weaker decrease in TD probability than
259 non-persistent WR-E. Persistent and non-persistent WR-C show TD probability anomalies of
260 opposite signs, both with a small magnitude. Compared to TD probability, the anomalies of TO
261 probability are generally stronger for both persistent WRs and non-persistent WRs. In particular,
262 persistent WR-B is associated with an increase of TO probability by close 80% and accounts for
263 about 30% of all TOs, while persistent WR-A is associated with a decrease of TO probability by
264 about 70%. However, a consistent picture emerges: persistent WRs amplify the positive
265 anomalies but do not further enhance the negative anomalies in comparison to the corresponding
266 non-persistent WRs. The exception is persistent WR-C, which is associated with nearly zero TO
267 anomaly, in contrast to a positive but not significant anomaly for non-persistent WR-C (Fig. 4b).

268 The asymmetric impacts of WR persistence on positive and negative tornado activity anomalies
269 are also illustrated in Fig. S2. One possible interpretation is that tornado activity indices are
270 positively defined metrics so they cannot be reduced much further when already close to zero.
271 Additionally, the results should also be interpreted with caution given the limited sample sizes
272 for certain groups (Table S1).



273

274 **Figure 4:** (a) TD and (b) TO (days with > 10 EF-1+ tornadoes) probability anomalies for each WR for persistent
275 and non-persistent days. Anomalies above the 95 % confidence based on the Monte Carlo testing are marked with an
276 asterisk. Anomalies above the 95 % confidence level based on the Monte Carlo testing (with 10,000 resampling) are
277 regarded as significant and marked with an asterisk.

278

279



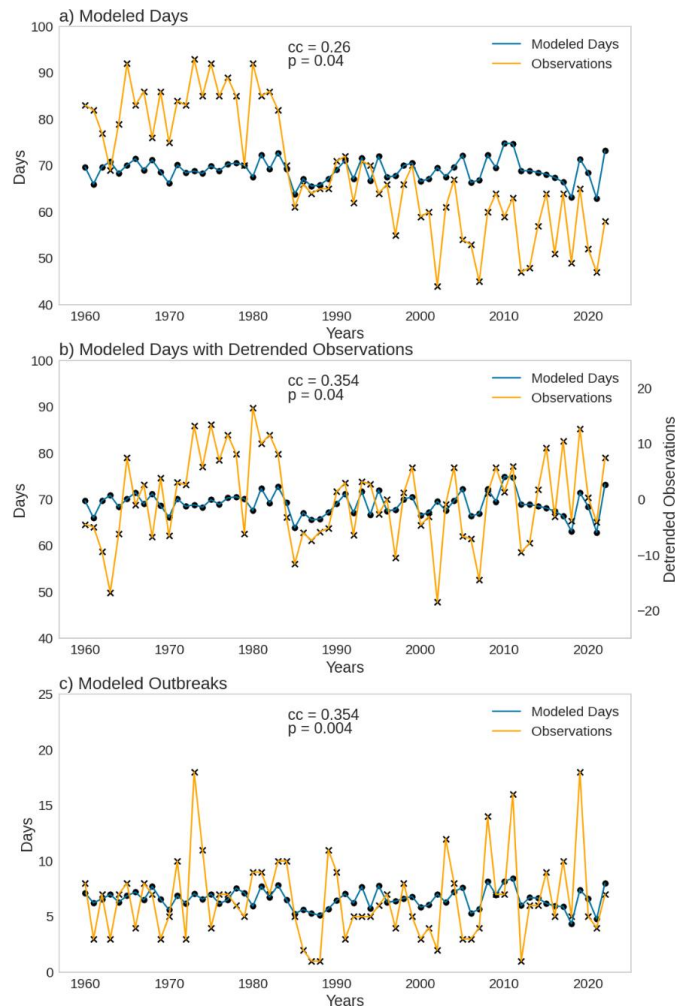
280 **4 Variability of WRs and Tornado Activity**

281 In this section, we further quantify the link between WRs and tornado activity. WR frequencies
282 demonstrate strong interannual and decadal variability (Fig. S4a-e). In particular, WR-A exhibits
283 a frequency increase during the 1980s and reached a peak around 1990, coinciding with the
284 steepest decrease in TDs (Brooks et al., 2014; Graber et al., 2024); and WR-D shows a negative
285 trend of occurrence in the recent two decades. The frequencies of persistent WRs also show
286 changes across different multidecadal time periods (Fig. S4f).

287 To examine whether WRs can help explain the interannual and decadal variability of tornado
288 activity over the period 1960-2022, an empirical model was developed following Eq. 2. Figure
289 5a shows the empirically modelled TDs along with the observed TDs. Despite the decadal
290 variability of WR and persistent WR frequencies (Fig. S4), the empirical model fails to capture
291 the observed decreasing trend or the decadal shift in the 1980s. After detrending the observations
292 using the least-squares fit, the model reasonably represents the interannual variability of TDs
293 (Fig. 5b), with a rank correlation of **0.35** (p-value ~ 0.04). An empirical framework for EF-3+
294 TDs was also tested, yielding a rank correlation of **0.37** (Fig. S5). It is interesting to note that the
295 modelled TDs are nearly out of phase with observations in the 1960s, when tornado reports are
296 less reliable (Trapp, 2013). After excluding these years, we reconstructed the empirical model
297 using updated TD probabilities during 1970-2022, and the correlation increases to **0.46** (Fig.
298 S6a). The empirical framework was also tested for EF-3+ TDs during 1970-2022, and the
299 correlation is **0.49** (Fig. S6b).

300 We also examined TOs. The empirical model picks up the interannual variability of the observed
301 TOs with a correlation of **0.36**, although the magnitude of the variability is underestimated (Fig.
302 6c), which is a typical limitation of statistical models. Since the observed TOs do not have a
303 strong trend, detrending the data does not affect the results appreciably. Similar to the TD model
304 results (Fig. 5a, b), the TO model is nearly out of phase with the observations in 1960s. After
305 excluding the data in 1960s, the correlation between the empirical model and observation
306 increases to **0.43** from 1970-2022 (Fig. S6c).

307



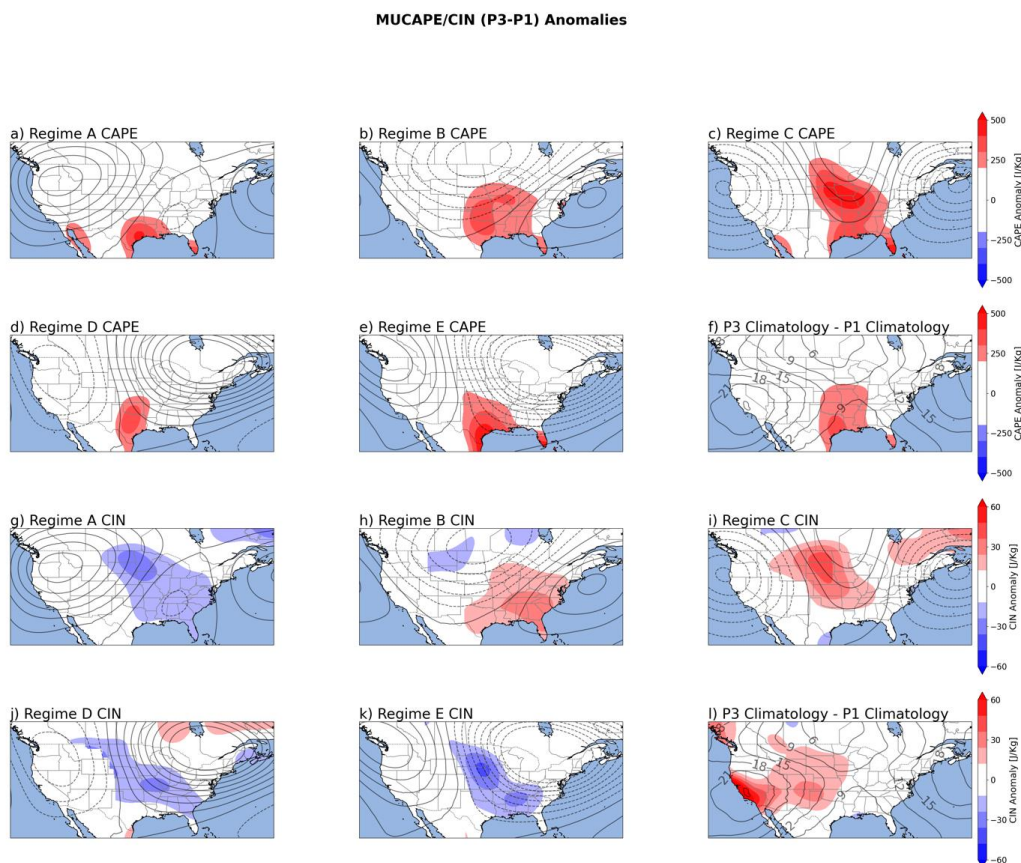
308

309 **Figure 5:** Empirically modeled TDs (blue) per year overlaid with (a) observed TDs (yellow) and (b) detrended
310 observed TDs (yellow) with spearman rank correlation coefficient (cc) and p-value; (c) empirically modeled (blue)
311 and observed (yellow) TOs per year with the spearman rank correlation coefficient and p-value.

312 It is worth noting that although the empirical model captures the interannual variability of TDs
313 reasonably well, it misses the negative trend or decadal variability of TDs. The empirical model
314 is constructed under the assumption that probability anomalies of tornado activity associated
315 with the WRs do not change during the period of analysis. This assumption, however, may not
316 be strictly valid. For example, MUCAPE increases over time for all five WRs, although S06
317 undergoes smaller changes (Fig. 6a-f, S7-S8). Additionally, convective inhibition (CIN)
318 increases in the Southeast for WR-B (Fig. 6h) and in the central-CONUS for WR-C (Fig. 6i)
319 from P1 to P3. Further analysis reveals lower TD probability for various regimes in P3 than in P1
320 (not shown). This may explain why the empirical model fails to capture the trend of TDs. A
321 better understanding of dynamic and thermodynamic anomalies associated with WRs and the



322 role of internal climate variability and anthropogenic forcing in modulating WRs will help us
323 better understand tornado activity on the decadal and longer time scales.



324

325 **Figure 6:** Change in MUCAPE (shading) anomalies (a-e) and CIN (shading) anomalies (g-k) from period 1 (1960-
326 1979) to period 3 (2000-2022) for each WR and (f, l) all WR days.

327 5. Summary

328 The weather regime concept was used to investigate the link between synoptic-scale circulation
329 patterns and the variability of tornado activity over the U.S. on the interannual time scale. Five
330 WRs were identified over North America using the K-means clustering analysis of daily 500H
331 anomalies from the ERA-5 reanalysis. WR-A is a three-cell wave-pattern and is associated with
332 negative anomalies of tornado activity in the central-CONUS, which is consistent with negative
333 anomalies of MUCAPE and S06 over that region. WR-B is a three-cell wave-pattern that
334 contributes to increased tornado activity in the Southeast as evidenced by positive anomalies in
335 MUCAPE and S06 there. WR-C is a three-cell wave-pattern with negative 500H anomalies over
336 both coasts. It is associated with positive MUCAPE anomalies over the central-CONUS and
337 negative S06 anomalies. It exhibits climatologically average tornado activity, but it does make a



338 positive, spatially small, contribution to tornado activity in the Great Plains. WR-D and WR-E
339 are both dipole patterns with positive and negative 500H anomalies over the east coast,
340 respectively. WR-D contributes to anomalously positive tornado activity in the Great Plains
341 while WR-E contributes to anomalously negative tornado activity in the Great Plains. WR-E also
342 contributes to positive anomalies of tornado activity in the Southeast, possibly linked to tropical
343 cyclones. A year that includes a high number of WR-B days is likely to have an above average
344 number of TDs and TOs. In contrast, a year with a high number of WR-A days would likely have
345 a below average number of TDs and TOs

346 We tested the hypothesis that WR persistence amplifies the tornado activity anomalies,
347 regardless of positive or negative anomalies. However, the impacts of WR persistence on
348 positive and negative tornado activity anomalies are found to be asymmetric: persistent WRs
349 amplify the positive anomalies but may not further enhance the negative anomalies. This can
350 probably be attributed to the positive-definite nature of tornado activity indices. While persistent
351 WRs with favorable environmental conditions (such as WRs B and D) may further increase
352 tornado activity, TD or TO probability cannot be reduced much further by the persistence of a
353 tornado-unfavorable WR (such as WR-A) when they are already close to zero.

354 Using WR frequency and persistence, an empirical model was developed to quantify the
355 relationship between tornado activity and warm-season WRs. The performance of the empirical
356 model shows promising skill in estimating the interannual variability of tornado days or TO
357 days, and the model performance was better after excluding the data in the 1960s. The empirical
358 model, however, misses the trend or the multi-decadal variability of TDs. This model deficiency
359 could be attributed to the non-stationary relationship between WRs and tornado activity on the
360 multi-decadal time scale, which is illustrated by the increase in CAPE for all WRs in the more
361 recent decades. The roles of internal variability and anthropogenic forcing, however, is outside
362 the scope of the present study and merit further investigation. Overall, weather regimes offer a
363 promising path for developing skillful seasonal tornado prediction models. Such efforts are
364 ongoing and will be reported in due course.

365

366

367

368

369

370

371

372

373

374



375 **Code Availability**

376 The codes used to reproduce this analysis will be made available in a github repository upon
377 publication.

378

379 **Data Availability**

380 The ERA5 data are available at the NCAR research data archive (RDA) (ds 633.0).

381 doi: 10.5065/BH6N-5N20

382 The tornado report data used in this study are available through the NOAA Storm Prediction
383 Center severe weather database.

384 <https://www.spc.noaa.gov/wcm/#data>

385

386 **Author Contributions**

387 Conceptualization: ZW, RJT, MG

388 Methodology: MG, ZW, RJT

389 Project Administration: RJT, ZW

390 Supervision: ZW, RJT

391 Writing – Original Draft: MG

392 Writing – Review and Edits: MG, ZW, RJT

393

394 **Competing Interests:**

395 Authors declare they have no competing interest.

396

397 **Acknowledgements**

398 We acknowledge the NCAR Computation and Information Systems Laboratory (CISL) for
399 providing computing resources through Derecho. All ERA5 data are available used in this study
400 are available at the research data archive. Tornado report data is available through the NOAA
401 Storm Prediction Center severe weather database.

402

403

404

405



406 **References**

- 407 Ashley, W. S. and Strader, S. M.: Recipe for Disaster: How the Dynamic Ingredients of Risk and Exposure
408 Are Changing the Tornado Disaster Landscape, *Bull. Am. Meteorol. Soc.*, 97, 767–786,
409 <https://doi.org/10.1175/BAMS-D-15-00150.1>, 2016.
- 410 Bieringer, P. and Ray, P. S.: A Comparison of Tornado Warning Lead Times with and without NEXRAD
411 Doppler Radar, *Weather Forecast.*, 11, 47–52, [https://doi.org/10.1175/1520-0434\(1996\)011<0047:ACOTWL>2.0.CO;2](https://doi.org/10.1175/1520-0434(1996)011<0047:ACOTWL>2.0.CO;2), 1996.
- 413 Brooks, H. E., Lee, J. W., and Craven, J. P.: The Spatial Distribution of Severe Thunderstorm and Tornado
414 Environments from Global Reanalysis Data, *Atmospheric Res.*, 67–68, 73–94,
415 [https://doi.org/10.1016/S0169-8095\(03\)00045-0](https://doi.org/10.1016/S0169-8095(03)00045-0), 2003.
- 416 Brooks, H. E., Carbin, G. W., and Marsh, P. T.: Increased Variability of Tornado Occurrence in the United
417 States, *Science*, 346, 349–352, <https://doi.org/10.1126/science.1257460>, 2014.
- 418 Charney, J. G. and DeVore, J. G.: Multiple Flow Equilibria in the Atmosphere and Blocking, *J. Atmospheric
419 Sci.*, 36, 1205–1216, [https://doi.org/10.1175/1520-0469\(1979\)036<1205:MFEITA>2.0.CO;2](https://doi.org/10.1175/1520-0469(1979)036<1205:MFEITA>2.0.CO;2), 1979.
- 420 Cook, A. R., Leslie, L., Parsons, D., and Schaefer, J.: The Impact of El Nino-Southern Oscillation (ENSO) on
421 Winter and Early Spring U.S. Tornado Outbreaks, *J. Appl. Meteorol. Climatol.*, 56, 2455–2478,
422 <https://doi.org/10.1175/JAMC-D-16-0249.1>, 2017.
- 423 Corti, S., Molteni, F., and Palmer, T. N.: Signature of Recent Climate Change in Frequencies of Natural
424 Atmospheric Circulation Regimes, *Nature*, 398, 799–802, <https://doi.org/10.1038/19745>, 1999.
- 425 Cwik, P., McPherson, R. A., Richman, M. B., and Mercer, A. E.: Climatology of 500-hPa Geopotential
426 Height Anomalies Associated with May Tornado Outbreaks in the United States., *Int. J. Climatol.*, 43,
427 893–913, <https://doi.org/10.1002/joc.7841>, 2022.
- 428 Del Genio, A. D., Yao, M.-S., and Jonas, J.: Will Moist Convection be Stronger in a Warmer Climate?,
429 *Geophys. Res. Lett.*, 34, <https://doi.org/10.1029/2007GL030525>, 2007.
- 430 Diffenbaugh, N. S., Scherer, M., and Trapp, R. J.: Robust Increases in Severe Thunderstorm Environments
431 in Response to Greenhouse Forcing, *Proc. Natl. Acad. Sci. U. S. A.*, 110, 16361–16366,
432 <https://doi.org/10.1073/pnas.1307758110>, 2013.
- 433 Geng, T., Jia, F., Cai, W., Wu, L., Gan, B., Jing, Z., Li, S., and McPhaden, M. J.: Increased Occurrences of
434 Consecutive La Nina events under Global Warming, *Nature*, 619, 774–781,
435 <https://doi.org/10.1038/s41586-023-06236-9>, 2023.
- 436 Gensini, V. A. and Brooks, H. E.: Spatial Trends in United States Tornado Frequency, *Nature*, 1,
437 <https://doi.org/10.1038/s41612-018-0048-2>, 2018.
- 438 Graber, M., Trapp, R. J., and Wang, Z.: The Regionality and Seasonality of Tornado Trends in the United
439 States, *Npj Clim. Atmospheric Sci.*, 7, <https://doi.org/10.1038/s41612-024-00698-y>, 2024.



- 440 Hannachi, A., Straus, D. M., Franzke, C. L. E., Corti, S., and Woollings, T.: Low-Frequency Nonlinearity and
441 Regime Behavior in the Northern Hemisphere Extratropical Atmosphere, *Rev. Geophys.*, 55, 199–234,
442 <https://doi.org/10.1002/2015RG000509>, 2017.
- 443 Hersbach, H., Bell, B., Berrisford, P., Hirahara, S., Horányi, A., Muñoz-Sabater, J., Nicolas, J., Peubey, C.,
444 Radu, R., Schepers, D., Simmons, A., Soci, C., Abdalla, S., Abellan, X., Balsamo, G., Bechtold, P., Biavati,
445 G., Bidlot, J., Bonavita, M., De Chiara, G., Dahlgren, P., Dee, D., Diamantakis, M., Dragani, R., Flemming,
446 J., Forbes, R., Fuentes, M., Geer, A., Haimberger, L., Healy, S., Hogan, R. J., Hólm, E., Janisková, M.,
447 Keeley, S., Laloyaux, P., Lopez, P., Lupu, C., Radnoti, G., de Rosnay, P., Rozum, I., Vamborg, F., Villaume,
448 S., and Thépaut, J.-N.: The ERA5 global reanalysis, *Q. J. R. Meteorol. Soc.*, 146, 1999–2049,
449 <https://doi.org/10.1002/qj.3803>, 2020.
- 450 Kodinariya, T. M. and Makwana, P. R.: Review on Determining Number of Clusters in K-Means
451 Clustering., *Int. J. Adv. Res. Comput. Sci. Manag. Stud.*, 1, 90–95, 2013.
- 452 Lee, S. H. and Messori, G.: The Dynamical Footprint of Year-Round North American Weather Regimes,
453 *Geophys. Res. Lett.*, 51, 2024.
- 454 Lee, S.-K., Wittenberg, A. T., Enfield, D. B., Weaver, S. J., Wang, C., and Atlas, R.: US Regional Tornado
455 Outbreaks and their Links to Spring ENSO Phases and North Atlantic SST Variability, *Environ. Res. Lett.*,
456 11, <https://doi.org/10.1088/1748-9326/11/4/044008>, 2016.
- 457 Mercer, A. E. and Bates, A.: Meteorological Differences Characterizing Tornado Outbreak Forecasts of
458 Varying Quality, *Atmosphere*, 1, 16, <https://doi.org/10.3390/atmos10010016>, 2019.
- 459 Mercer, A. E., Shafer, C. M., Doswell III, C. A., Leslie, L. M., and Richman, M. B.: Synoptic Composites of
460 Tornadoic and Nontornadoic Outbreaks, *Mon. Weather Rev.*, 140, 2590–2608,
461 <https://doi.org/10.1175/MWR-D-12-00029.1>, 2012.
- 462 Michelangeli, P.-A., Vautard, R., and Legras, B.: Weather Regimes: Recurrence and Quasi Stationarity, *J.*
463 *Atmospheric Sci.*, 52, 1237–1256, [https://doi.org/10.1175/1520-0469\(1995\)052%3C1237:WRRAS%3E2.0.CO;2](https://doi.org/10.1175/1520-0469(1995)052%3C1237:WRRAS%3E2.0.CO;2), 1995.
- 465 Miller, D., Wang, Z., Trapp, R. J., and Harnos, D. S.: Hybrid Prediction of Weekly Tornado Activity Out to
466 Week 3: Utilizing Weather Regimes, *Geophys. Res. Lett.*, 47, <https://doi.org/10.1029/2020GL087253>,
467 2020.
- 468 Miller, D., Gensini, V. A., and Barrett, B. S.: Madden-Julian Oscillation Influences United States
469 Springtime Tornado and Hail Frequency, *Npj Clim. Atmospheric Sci.*, 5, <https://doi.org/10.1038/s41612-022-00263-5>, 2022.
- 471 Moore, T. W.: Annual and Seasonal Tornado Trends in the Contiguous United States and its Regions, *Int.*
472 *J. Climatol.*, 38, 1582–1594, <https://doi.org/10.1002/joc.5285>, 2018.
- 473 Moore, T. W. and DeBoer, T. A.: A Review and Analysis of Possible Changes to the Climatology of
474 Tornadoes in the United States, *Prog. Phys. Geogr. Earth Environ.*, 43,
475 <https://doi.org/10.1177/0309133319829398>, 2019.
- 476 NCEI: U.S. Billion-Dollar Weather and Climate Disasters, 2024.



- 477 Niloufar, N., Devineni, N., Were, V., and Khanbilvardi, R.: Explaining the Trends and Variability in the
478 United States Tornado Records using Climate Teleconnections and Shifts in Observational Practices, *Sci.*
479 *Rep.*, 11, <https://doi.org/10.1038/s41598-021-81143-5>, 2021.
- 480 Rasmussen, E. N. and Blanchard, D. O.: A Baseline Climatology of Sounding-Serived Supercell and
481 Tornado Forecast Parameters., *Weather Forecast.*, 13, 1148–1164, [https://doi.org/10.1175/1520-0434\(1998\)013<1148:ABCOSD>2.0.CO;2](https://doi.org/10.1175/1520-0434(1998)013<1148:ABCOSD>2.0.CO;2), 1998.
- 483 Storm Prediction Center: U.S. Killer Tornado Statistics, 2024.
- 484 Strader, S. M., Ashley, W. S., Pingel, T. J., and Krmenc, A. J.: Projected 21st Century Changes in Tornado
485 Exposure, Risk, and Disaster Potential, *Clim. Change*, 141, 301–313, <https://doi.org/10.1007/s10584-017-1905-4>, 2017.
- 487 Strader, S. M., Gensini, V. A., Ashley, W. S., and Wagner, A. N.: Changes in Tornado risk and Societal
488 Vulnerability Leading to Greater Tornado Impact Potential, *Npj Nat. Hazards*, 1, 2024.
- 489 Thompson, D. B. and Roundy, P. E.: The Relationship between the Madden-Julian Oscillation and US
490 Violent Tornado Outbreaks in the Spring, *Mon. Weather Rev.*, 141, 2087–2095,
491 <https://doi.org/10.1175/MWR-D-12-00173.1>, 1998.
- 492 Thompson, R. L., Smith, B. T., Grams, J. S., Dean, A. R., and Broyles, C.: Convective Modes for Significant
493 Severe Thunderstorms in the Contiguous United States. Part II: Supercell and QLCS Tornado
494 Environments, *Weather Forecast.*, 27, 1136–1154, <https://doi.org/10.1175/WAF-D-11-00116.1>, 2012.
- 495 Tippett, M. K.: Changing Volatility of U.S. Annual Tornado Reports, *Geophys. Res. Lett.*, 41, 6956–6961,
496 <https://doi.org/10.1002/2014GL061347>, 2014.
- 497 Tippett, M. K., Sobel, A. H., Camargo, S. J., and Allen, J. T.: An Empirical Relation between U.S. Tornado
498 Activity and Monthly Environmental Parameters, *J. Clim.*, 27, 2983–2999, <https://doi.org/10.1175/JCLI-D-13-00345.1>, 2014.
- 500 Tippett, M. K., Lepore, C., and L’Heureux, M. L.: Predictability of a Tornado Environment Index from El
501 Nino Southern Oscillation (ENSO) and the Arctic Oscillation, *Weather Clim. Dyn.*, 3, 1063–1075,
502 <https://doi.org/10.5194/wcd-3-1063-2022>, 2022.
- 503 Tippett, M. K., Malloy, K., and Lee, S. H.: Modulation of U.S. Tornado Activity by year-round North
504 American Weather Regimes, *Mon. Weather Rev.*, <https://doi.org/10.1175/MWR-D-24-0016.1>, 2024.
- 505 Trapp, R. J.: *Mesoscale-Convective Processes in the Atmosphere*, Cambridge University Press, 2013.
- 506 Trapp, R. J.: On the Significance of Multiple Consecutive Days of Tornado Activity, *Mon. Weather Rev.*,
507 142, 1452–1459, <https://doi.org/10.1175/MWR-D-13-00347.1>, 2014.
- 508 Trapp, R. J., Diffenbaugh, N. S., Brooks, H. E., Baldwin, M. E., Robinson, E. D., and Pal, J. S.: Changes in
509 Severe Thunderstorm Environment Frequency during the 21st Century caused by Anthropogenically
510 Enhanced Global Radiative Forcing, *Proc. Natl. Acad. Sci. U. S. A.*, 104, 19719–19723,
511 <https://doi.org/10.1073/pnas.0705494104>, 2007.



512 Vigaud, N., Tippett, M. K., and Robertson, A. W.: Probabilistic Skill of Subseasonal Precipitation Forecasts
513 for the East Africa-West Asia Sector during September-May, *Weather Forecast.*, 33, 1513–1532,
514 <https://doi.org/10.1175/WAF-D-18-0074.1>, 2018.

515 Wakimoto, R. M. and Wilson, J. W.: Non-supercell Tornadoes, *Mon. Weather Rev.*, 117, 1113–1140,
516 [https://doi.org/10.1175/1520-0493\(1989\)117<1113:NST>2.0.CO;2](https://doi.org/10.1175/1520-0493(1989)117<1113:NST>2.0.CO;2), 1989.

517